Electronic Supplementary Materials

High-performance room-temperature NO_2 gas sensors enabled by 0D SnO_2/1D WO_3 heterostructures for wearable applications

Xiaohong Jiang[a, 1], Zhimin Guo[a, 1], Shiqun Zhang[a], Leilei Jia[a], Yawei Wang[a], Xinrui Zeng[a], Yaxin Lei[a], Hanbin Liu[a], Guodong Liu[a], Zhijian Li[a], Wenliang Zhang[a, *], Zhibin Lei[b, *]

[a] *College of Bioresource Chemical and Materials Engineering, Shaanxi University of Science & Technology, Xi'an, P.R. China (710021)*

[b] *Key Laboratory of Applied Surface and Colloid Chemistry, MOE, Shaanxi Engineering Lab for Advanced Energy Technology, Shaanxi Key Laboratory for Advanced Energy Devices, School of Materials Science and Engineering, Shaanxi Normal University, 620 West Chang'an Street, Xi'an, P.R. China (710119)*

[1] These authors contributed equally to this work.

[*] Correspondence: W. L. Zhang, E-mail: wlzhang@sust.edu.cn;

Z. B. Lei, E-mail: zblei@snnu.edu.cn

Gas-cell flow/pressure, mixing, and purge protocols.

Purging and cleaning protocol. This protocol is executed prior to each introduction of a new gas or repetitive cycling test to establish a clean and reliable measurement baseline. Operational Steps: Switch the gas path of the system to the diluent gas (typically synthetic air or N_2). Set the total flow rate to a predetermined value. Continue purging until the sensor's electrical signal stabilizes at a constant value (with a variation rate of less than 1% per minute), indicating that the test chamber and sensor surface have reached a clean and stable state ready for testing.

Gas mixing and flow control protocol. The desired target gas concentration is generated using the dynamic volumetric mixing method, with the specific calculation formula as follows:

$$C_{target} = (F_{analyte} \times C_{parent}) / F_{total}$$

Where: C_{target} is the desired target gas concentration (unit: ppm). $F_{analyte}$ is the flow rate of the analyte parent gas through its MFC (unit: sccm). C_{parent} is the concentration of the analyte parent gas itself (unit: ppm). F_{total} is the total gas flow rate (unit: sccm), calculated as $F_{total} = F_{analyte} + F_{diluent}$.

Flow and pressure control protocol. Flow Control: All experiments were conducted under a constant total flow rate. The flow rates used in this study ranged between 100-500 sccm, with specific values determined by the experimental design. This ensured consistent hydrodynamic conditions and gas residence times across different test batches.

Pressure control: The entire test system operated with the chamber outlet venting directly to the atmosphere. By precisely controlling the inlet flow rate, the system naturally maintained a stable slight positive pressure inside the test chamber, slightly above ambient atmospheric pressure. This design effectively prevents the diffusion of external air into the chamber, thereby ensuring the purity and consistency of the test atmosphere.

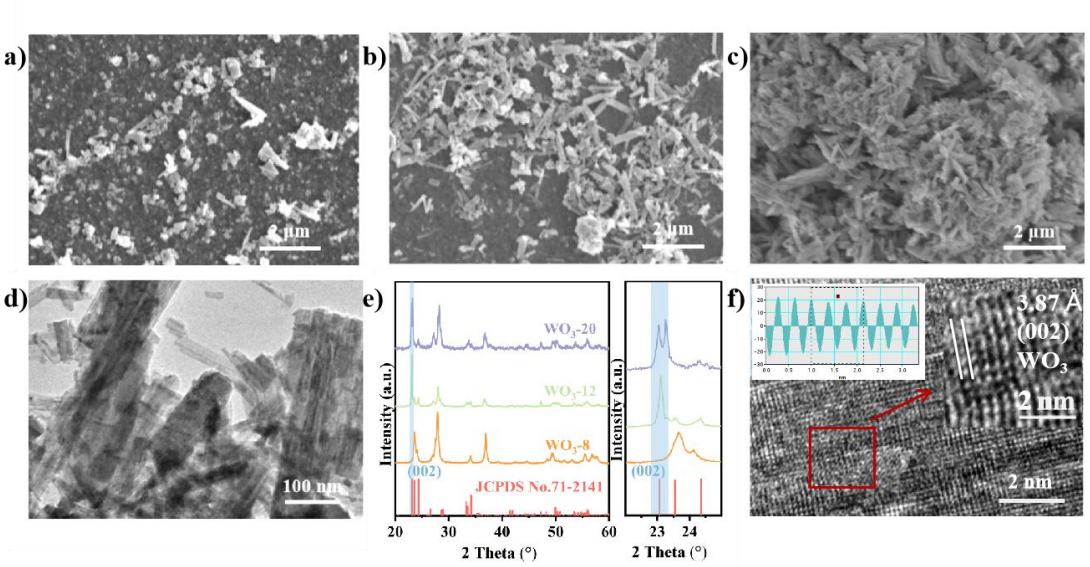

Figure S1. (a-c) SEM images of WO_3-8, WO_3-12, and WO_3-20, respectively, (d) XRD images of WO_3-8, WO_3-12, and WO_3-20, (e) TEM and (f) HRTEM images of WO_3-12, inset: The IFFT image of WO_3-12.

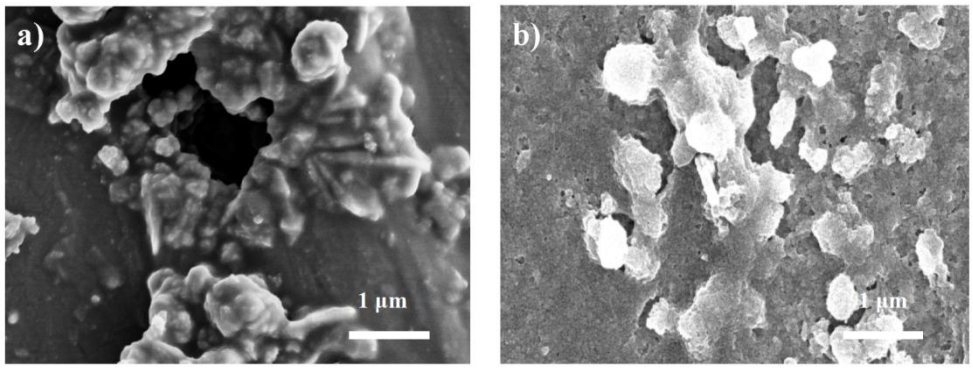

Figure S2. SEM images of (a) Sn/W-O-10 and (b) Sn/W-O-14.

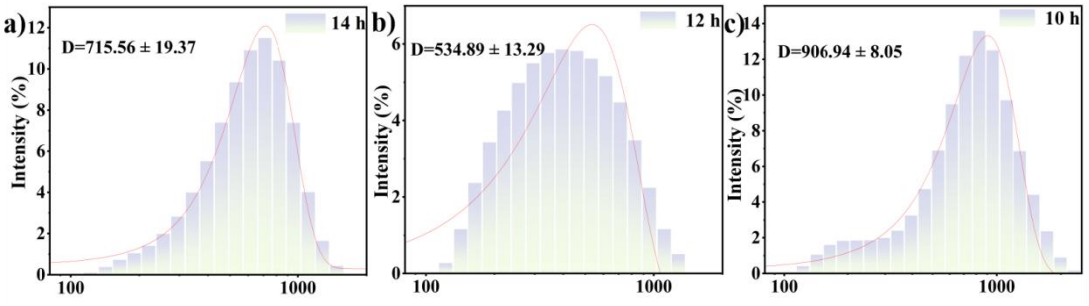

Figure S3. (a-c) Size distribution of (a) Sn/W-O-14, (b) Sn/W-O-12, and (c) Sn/W-O-10.

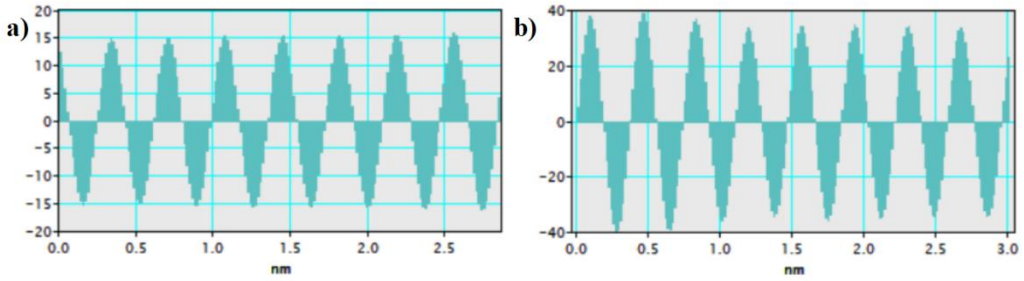

Figure S4. The IFFT images of (a) WO_3 and (b) SnO_2.

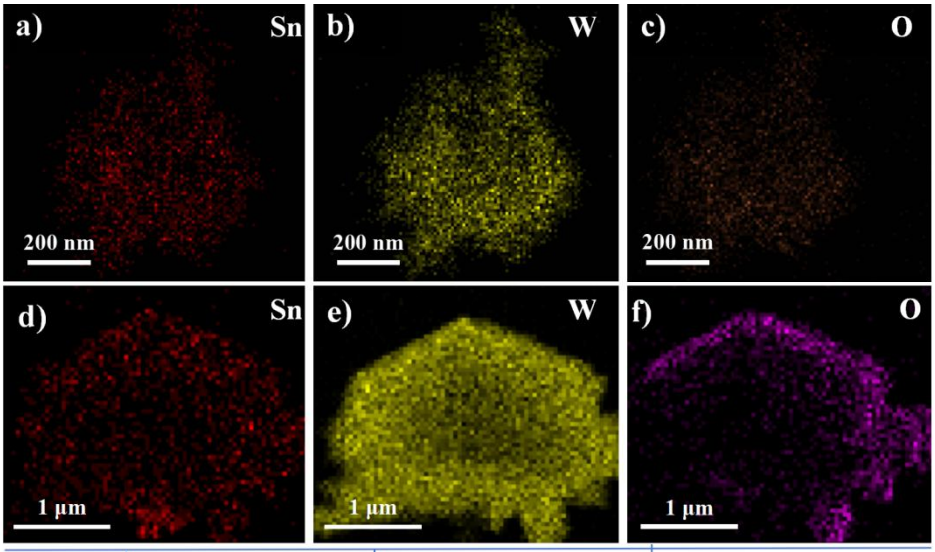

g)

Element	Atomic % (Sn/W-O-14)	Atomic % (Sn/W-O-12)	Atomic % (Sn/W-O-10)
O K	35.03	97.19	59.75
Sn L	23.96	0.41	2.13
W L	31.93	2.40	38.12

Figure S5. (a-f) EDX mapping images of Sn/W-O-14 (a-c) and Sn/W-O-10 (d-f), (g) variation of the contents of Sn, W, and O elements in Sn/W-O-14, Sn/W-O-12 and Sn/W-O-10.

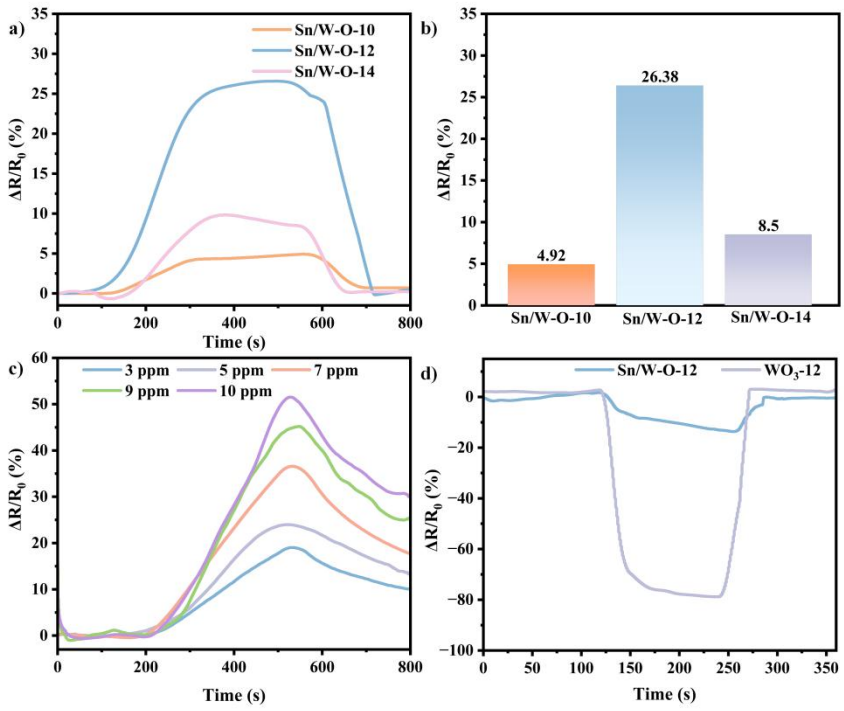

Figure S6. (a) Response and recovery curves of Sn/W-O-10, Sn/W-O-12, Sn/W-O-14 sensors under 5.0 ppm NO_2 at room temperature (RT), (b) bar graph of the maximum response value of Sn/W-O-10, Sn/W-O-12, and Sn/W-O-14 sensors from (a), (c) response and recovery curves of WO_3-12 under 3-10 ppm of NO_2, (d) response and recovery curves of WO_3 and Sn/W-O-12 at 50% relative humidity (RH).

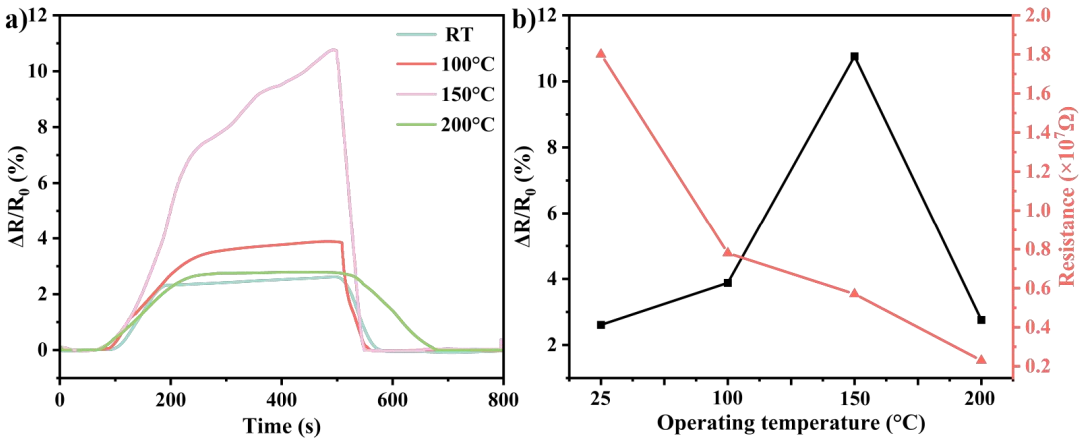

Figure S7. (a) Response–temperature curves of the Sn/W-O-12 sensor to 0.8 ppm NO_2 at different operating temperatures, (b) initial resistances and sensor responses of the Sn/W-O-12 sensor measured at different operating temperatures.

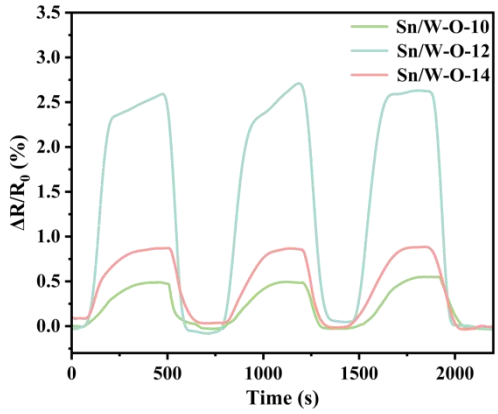

Figure S8. Cycling stability curves of Sn/W-O-10, Sn/W-O-12, Sn/W-O-14 sensors to 0.8 ppm NO_2.

Table S1: Comparison of gas sensing performance of Sn/W-O-12 with other reported materials.

Materials	T (K)	Long-term stability (days) (Keep > 90% initial value)	Response/Recovery times (s)	LOD (ppm)	Response (%)	Ref.
CuO/rGO	333	10	1250/1800	/	4.8 (0.02 ppm)	[1]
MoS_2/graphene	498	/	0.7/0.9	0.2	29.8 (1.0 ppm)	[2]
MoS_2/SnO_2	298	14	530/680	/	0.6 (0.5 ppm)	[3]
g-C_3N_4/GaN	478	30	72/145	/	229 (10.0 ppm)	[4]
NbS_2	298	/	5000/7000	0.241	15.0 (5.0 ppm)	[5]
SnS_2@c-MOF	298	35	206/248	1.0	8.29 (10.0 ppm)	[6]
Au/MoS_2	298	28	75/90	0.025	0.3 (2.5 ppm)	[7]
In_2O_3-ZnO NWs	478	70	15/45	/	13.0 (4.0 ppm)	[8]
NW-Au	498	/	170/260	/	9.0 (20.0 ppm)	[9]
ZnO/In_2O_3	298	30	35/250	1.0	2.21 (5.0 ppm)	[10]
Sn/W-O-12	298	60	63/38 (0.8 ppm); 169/96 (5.0 ppm)	0.218	2.36 (0.8 ppm); 23.43 (0.8 ppm)	This work

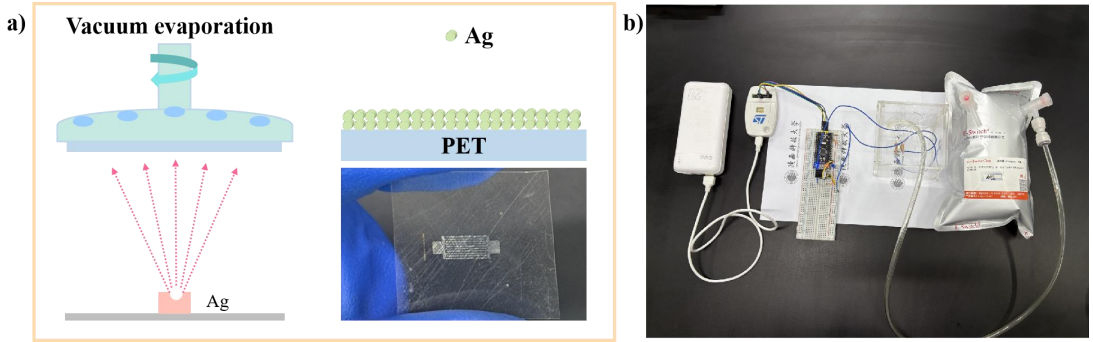

Figure S9. (a) Schematic illustration of the synthesis process for the flexible NO_2 gas sensor based on Sn/W-O-12, (b) schematic diagram of the homemade dynamic testing platform, which includes a stm32f103cbt6 minimal system board mounted on a breadboard, along with a buzzer and an LED.

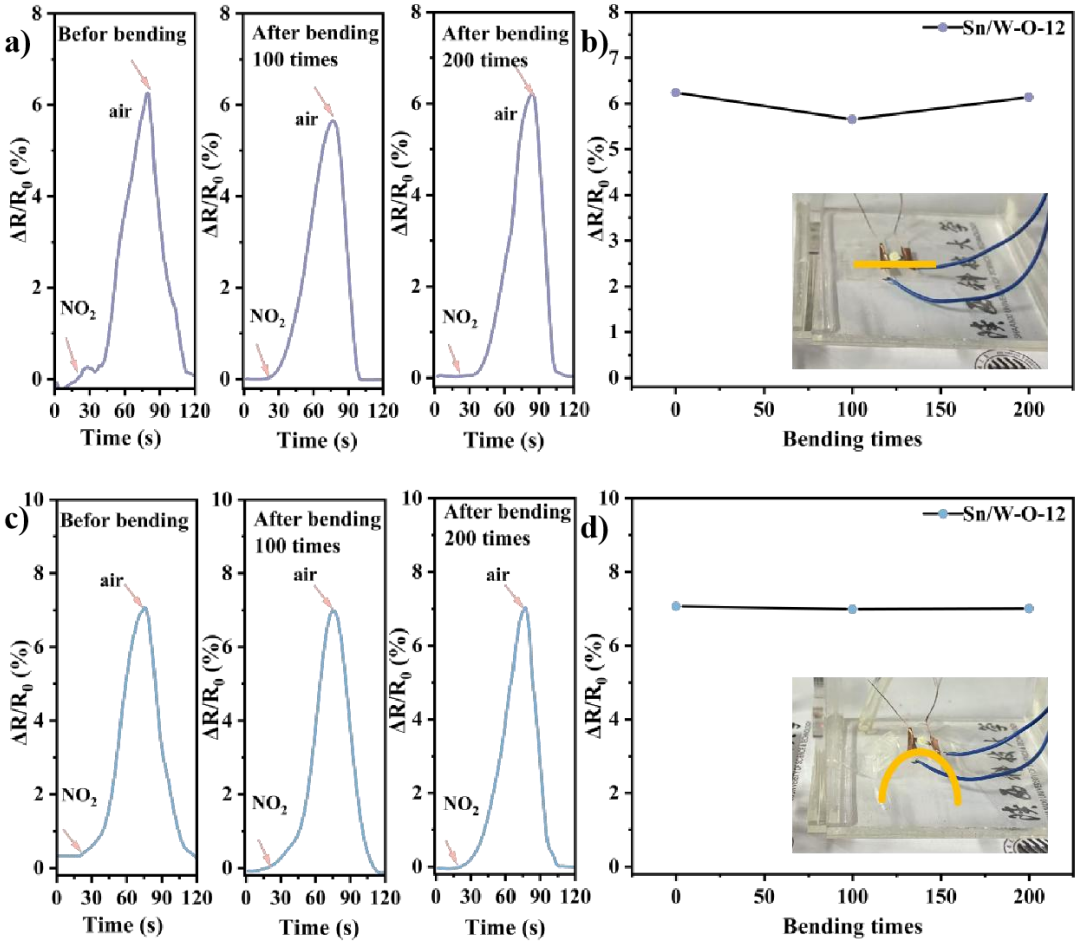

Figure S10. Dynamic gas sensing characteristics of the flexible Sn/W-O-12 gas sensor for 2 ppm NO_2 gas at (a, b) flat and (c, d) bend conditions.

References

1. Y. Zhou, G. Liu, X. Zhu and Y. Guo, *Ceramics International*, 2017, **43**, 8372-8377.
2. H. S. Hong, N. H. Phuong, N. T. Huong, N. H. Nam and N. T. Hue, *Applied Surface Science*, 2019, **492**, 449-454.
3. Y. Han, Y. Ma, Y. Liu, S. Xu, X. Chen, M. Zeng, N. Hu, Y. Su, Z. Zhou and Z. Yang, *Applied Surface Science*, 2019, **493**, 613-619.
4. D. Simon Patrick, A. Govind, P. Bharathi, M. Krishna Mohan, S. Harish, J. Archana and M. Navaneethan, *Applied Surface Science*, 2023, **609**, 155337.
5. Y. Kim, K. C. Kwon, S. Kang, C. Kim, T. H. Kim, S.-P. Hong, S. Y. Park, J. M. Suh, M.-J. Choi, S. Han and H. W. Jang, *ACS Sensors*, 2019, **4**, 2395-2402.
6. H. Xu, X. Cui, X. Qiu, W. Zeng and Q. Zhou, *Materials Today Chemistry*, 2025, **49**, 103024.
7. J. Hu, Y. Zhao, B. Liu and Y. Zhang, *Sensors and Actuators B: Chemical*, 2025, **433**, 137556.
8. E. Espid and F. Taghipour, *Sensors and Actuators B: Chemical*, 2017, **241**, 828-839.
9. M. Bonyani, S. Mojtaba Zebarjad, M. Kanani, M. Moaddeli, H. W. Kim and S. S. Kim, *Applied Surface Science*, 2024, **657**, 159773.

10. D. Goyal, D. V. Rupnar, A. Sapre, S. Samanta, N. S. Rawat, S. Bhattacharya, M. Kaur and N. S. Ramgir, *Journal of Alloys and Compounds Communications*, 2024, **4**, 100045.